ORIGINAL ARTICLE

Improving forming accuracy of variable-diameter tube by electromagnetic forming using segmented coil

Changxing Li[1] · Xiaofei Xu[2] · Shaowei Ouyang[1] · Limeng Du[1] · Wang Zhang[1] · Xinhui Zhu[1] · Xiaotao Han[1] · Quanliang Cao[1] · Liang Li[1]

Abstract

Electromagnetic forming (EMF) has shown considerable promise in lightweight alloy tube manufacturing industry. However, the generated force field falls short of meeting the stringent forming accuracy requirements for variable-diameter tubes. To solve this, this paper proposes an EMF process using a novel coil structure, named as segmented coil, to improve the forming quality of tubes. The design and implementation of coil, as well as the deformation behavior of tubes, are discussed. Results show that a multi-layer solenoid coil can generate excessive force on the upper portion of the tube, thus causing an undesired gap between the coil and tube that is unfavorable for forming performance. In contrast, when employing a segmented coil, the force applied to this section is mitigated, allowing the tube to fit into the die from bottom to top and achieving a maximum die-fitting gap of no more than 0.1 mm. Besides, it is found that the forming accuracy increases with increasing discharge energy, and an optimal coil structure exists when the discharge energy is fixed. This work showcases the considerable flexibility of the segmented coil in controlling the Lorentz force distribution and tube deformation behavior. These findings hold significant implications for expanding the applications of EMF technology.

Keywords Deformation behavior · Electromagnetic forming · Lorentz force · Segmented coil · Variable-diameter tube

1 Introduction

The aluminum alloy variable-diameter tube finds extensive usage in the field of piping engineering, which serves the capability of facilitating piping connections and regulating fluid velocity [1]. Nonetheless, aluminum alloys exhibit limited formability at room temperature, easily resulting in cracks in the tube when the conventional cold extrusion process is applied.

Electromagnetic forming (EMF), as a specialized manufacturing technology based on pulsed Lorentz force,

possesses characteristics such as non-contact operation and high forming speed, which can enhance the formability limits and suppress wrinkling and springback of aluminum alloy materials [2–4]. For instance, Xiao et al. [5] reported that a 68.3% increase in forming limit and a 9.4% increase in hardness for AA1060-H24 sheets when electromagnetic forming (EMF) is applied compared to quasi-static stamping. Liu et al. [6] found that electromagnetic forming improved the forming limits of AA5182 O sheet by 43% under uniaxial tension, 53% under plane strain, and 59% under equal-biaxial tension compared to quasi-static forming. Cui et al. [7] demonstrated that the springback of an AA5052-O aluminum-alloy U-shape sheet can be significantly reduced when employing EMF, which can be ascribed to the decrease of tangential stress on the sheet corner. These studies demonstrate the feasibility of achieving high forming quality of aluminum alloy variable-diameter tubes using electromagnetic forming technology.

But unfortunately, previous research has shown that the Lorentz force distribution generated by a conventional coil fails to meet the force-field requirement of a variable-diameter tube, leading to subpar forming accuracy [8]. This

✉ Shaowei Ouyang
swouyang@hust.edu.cn

✉ Liang Li
liangli44@mail.hust.edu.cn

1   Wuhan National High Magnetic Field Center, Huazhong University of Science and Technology, Wuhan 430074, China

2   School of Materials Science and Engineering, Hubei University of Automotive Technology, Shiyan 442002, Hubei, China

limitation stems from the fact that the Lorentz force distribution is difficult to control during the electromagnetic forming since it tends to be concentrated within the area covered by the coil wires. As a consequence, it leads to typical concave deformations in both sheet [9–11] and tube [12–14] during free bulging processes, as well as poor forming accuracy during die-fitting processes [15].

To solve this, scholars have proposed a variety of new approaches to control the force, such as developing new coil structure, introducing intermediate media between coil and workpiece [16–18], and employing multiple coils and power sources [19–21], among which the use of a novel coil structure is effective and easy to implement. For example, regarding sheet forming, Kamal et al. [22] designed a uniform pressure actor (UPA) structure to induce an even Lorentz force across the sheet, which is achieved by incorporating a conductive channel located external to the coil. Building on this idea, Wu et al. [23] developed an improved UPA structure with the conductive channel placed inside the coil, leading to enhanced electrical contact and forming efficiency. Oliveira et al. [24] reported that the influence of dead spots can be avoid by employing a double spiral coil, thereby obtaining a more evenly distributed pressure on the sheet. Cui et al. [25] designed a flat spiral coil, known as the runway coil, to make pure aluminum sheet uniaxially tensioned by EMF. Regarding tube forming, Soni et al. [26] demonstrated that the coil parameters like inner diameter, outer diameter, effective number of turns have significant effects on the forming performance of tubes. Qiu et al. [27] suggested a concave coil structure to improve the uniformity of the tube, incorporating a reduced number of turns in the middle section of the coil. Ouyang et al. [28] split a conventional coil into three sub-coils to realize different forming shapes of tubes, but the complex power supply equipment limits its wide application. Li et al. [8] developed a sectional coil constructed by varying coil spacing to enhance variable-diameter tubes' forming performance. This work is innovative and works, but it is only applicable to single-layer coil that suffers poor forming efficiency.

In summary, designing new coil structures has been a trend in the area of EMF research since the coil's geometry significantly influences Lorentz force distribution, which consequently affects the deformation process and final forming performance of the workpiece. However, according to the above-mentioned research, the developed coil structure especially for tube forming still has some inherent limitations. In this work, a new coil structure, named segmented coil, is developed to meet the force-field demands essential for the realization of high forming quality of AA6061-O variable-diameter tubes, aiming to offer a new force-regulation tool that is easy to implement in electromagnetic tube forming. In the following section, both numerical and experimental methods are first performed to verify the effectiveness of the proposed coil, and then the tube deformation behavior is studied.

2 Principle and method

2.1 Principle

Figure 1a displays the schematic of variable-diameter tubes deformed by electromagnetic method, comprising the forming coil, tube, die, and power supply. When the capacitor is triggered, a strong pulsed current will be generated in the coil, resulting in the creation of a magnetic field and eddy current in the tube. Subsequently, a pulsed Lorentz force is generated on the tube, forcing it to deform and match the die's shape. The expression for the Lorentz force density can be stated as follows:

$$F_r = J_{phi} \times B_z \tag{1}$$

$$F_z = J_{phi} \times B_r \tag{2}$$

where J_{phi} represents the induced eddy current density, while B_z and B_r denote the axial and radial magnetic flux density; F_r and F_z correspond to radial and axial Lorentz force density, respectively. Note that Fr serves as the primary driving force in tube forming. However, the Lorentz force generated by a traditional solenoid coil cannot be applied to achieve precise shaping of variable-diameter tubes because of its unreasonable distribution. Specifically, the length of the coil used to form a variable-diameter tube is commonly higher than that of the tube, leading to a greater force in the upper part of the tube, mainly due to the eddy current's end effect, which causes this section to make contact with the die first. Consequently, a gap forms between the tube and the die. During the experiment, it was observed that the air trapped in this gap could not escape, preventing further deformation of the tube [29]. This, in turn, results in poor forming accuracy of the final deformation shape, as illustrated in Fig. 1b.

A preferred method for shaping the variable-diameter tube involves ensuring that the tube can smoothly match the die from its bottom to the top. This allows for a reduction in the force acting on the upper portion of the tube, as illustrated in Fig. 2. In accordance with the Biot-Savart Law, the magnetic field density produced by a coil with multiple turns can be represented as follows:

$$\vec{B} = \sum_{i=1}^{n} \frac{\mu_0}{4\pi} \int_L \frac{Idl \times \vec{r}}{r^3} \tag{3}$$

Fig. 1 Schematic of the EMF system (**a**) and forming process (**b**) for variable-diameter tube
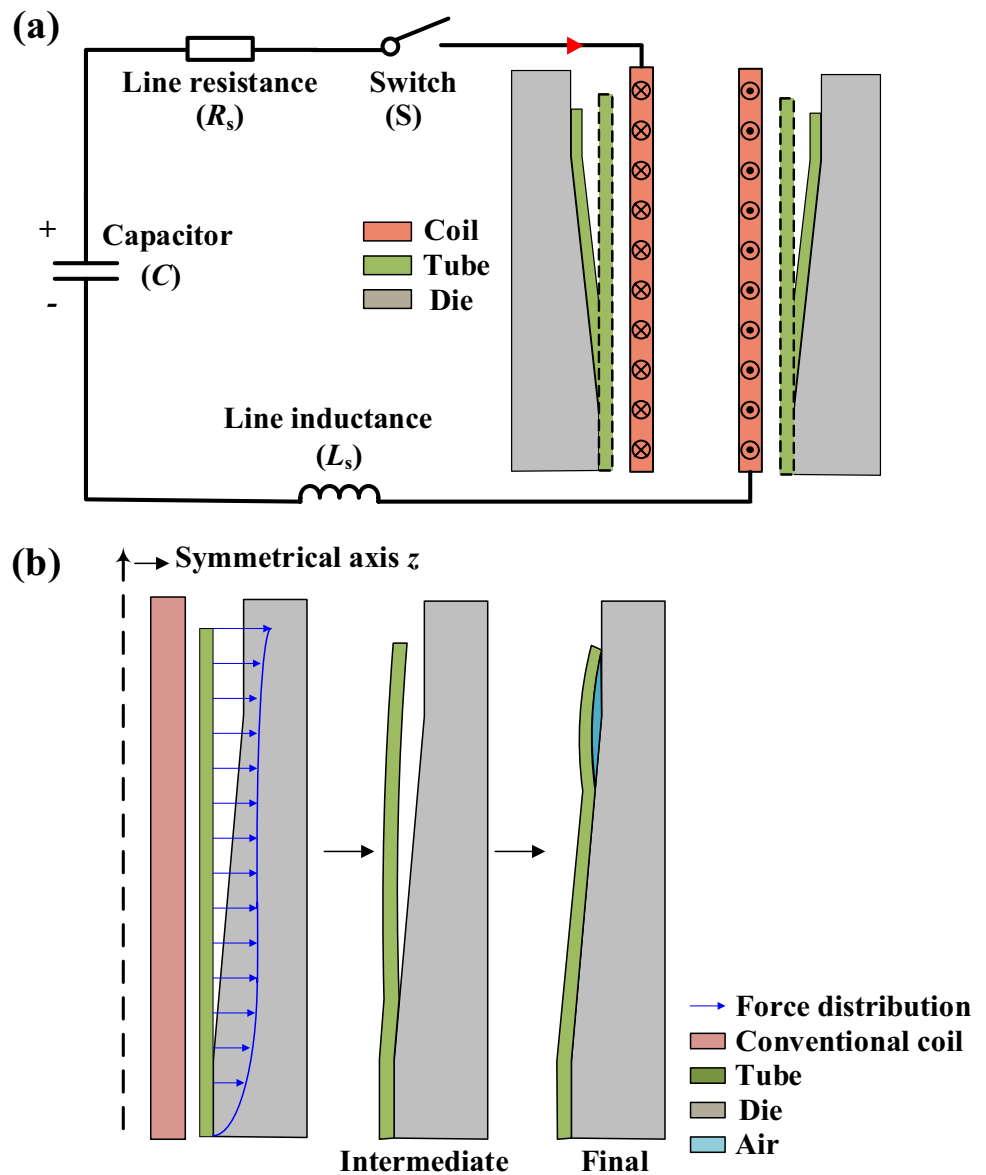
where I represents the current, dl stands for the tiny line element of the current, L denotes the integration path, n signifies the number of coil turns, and r represents the distance from the current element to the measurement point. It is evident that the magnetic field strength is affected by both the number of coil turns and the distance between the coil and tube. Consequently, the Lorentz force is able to be reduced by either decreasing coil turns or increasing the distance between the coil and tube. With this in mind, a segmented coil structure was developed, where the wire turns on the upper part of the coil is reduced, thereby decreasing the force on the upper portion of the tubes.

2.2 Geometric configuration

Figure 3a provides the geometric characteristics of the tube and die, where a tube made of AA6061-O aluminum alloy having a 2 mm thickness, a 76 mm diameter, and a 100 mm length was employed, along with a 304 steel die with a top hole of 96 mm and a bottom hole of 80 mm. The conventional solenoid coil composed of a single layer has been proven to cause poor forming accuracy of variable-diameter tubes by previous works [8, 29], while the applicability of this conclusion in multi-layer solenoid coils requires further verification considering that the number of coil turns could also affect the distribution of Lorentz force.

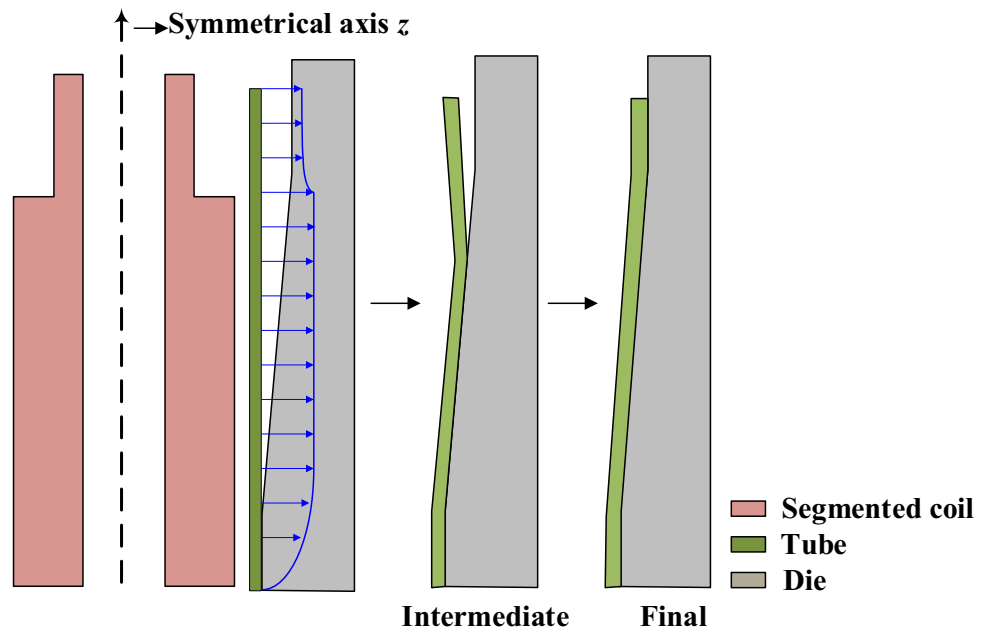**Fig. 2** Schematic of the tube-forming process by a segmented coil

Segmented coil
Tube
Die

Table 1 Main discharge parameters of the coils

Parameters	Conventional coil	Segmented coil
Total turns	96	90
Spacing between turns	0.5 mm	0.5 mm
Copper size	1×4 mm^2	1×4 mm^2
Inner diameter	58 mm	58 mm
Outer diameter	69 mm	69 mm

Figure 3b provides details regarding the structure parameters of the used solenoid coil, which was constructed using 96 turns of copper conductors arranged into 4 layers with a

rectangular cross-section measuring 1×4 mm^2. Figure 3c shows the developed segmented coil, where 6 turns of wire arranged into 2 layers near the upper portion of the coil are reduced compared to that in the conventional coil. More details regarding the coil structure are given in Table 1. The forming processes of tubes under a conventional coil and segmented coil are both discussed in this paper.

2.3 Discharge circuit

The equivalent circuit for the EMF process employing a segmented coil is depicted in Fig. 4. In this circuit, the coil and tube are represented as a connection of an

Fig. 3 Geometric parameter of the tube and die (**a**), the conventional coil (**b**), and the developed segmented coil (**c**)
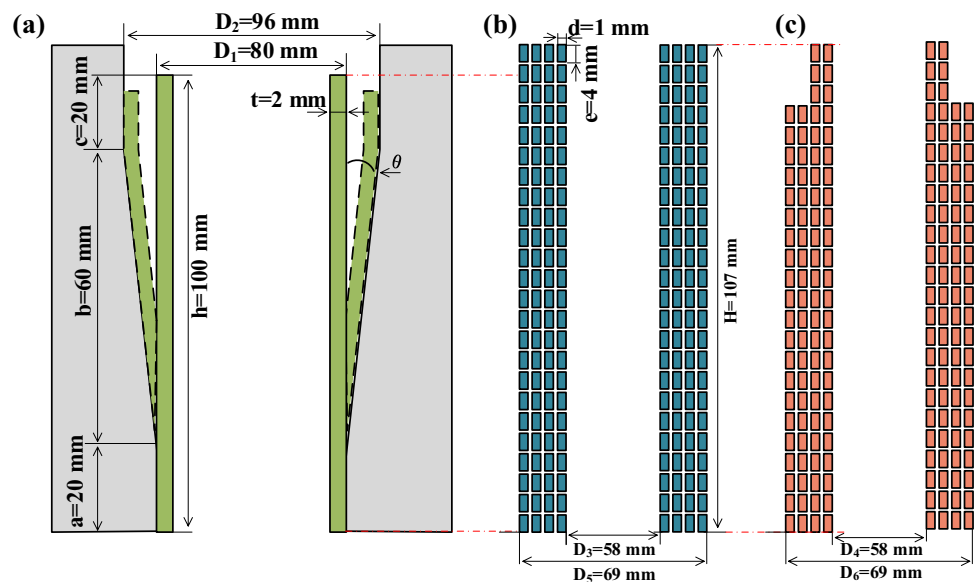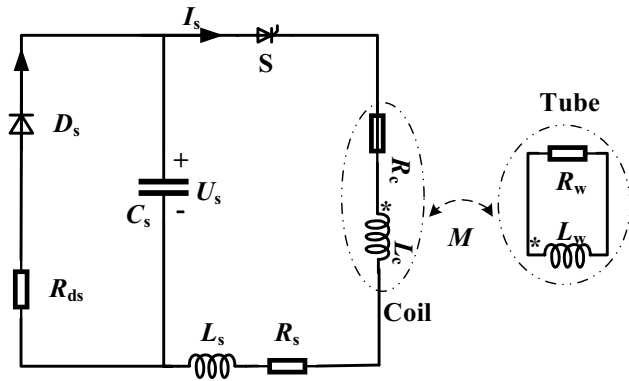
Fig. 4 Equivalent circuit for the EMF system using a segmented coil

Table 2 The primary circuit parameters in EMF system

Parameters	Symbol/unit	Value
Capacitance	$C_s/\mu F$	160
Line inductance	$L_s/\mu H$	7
Line resistance	$R_s/m\Omega$	7
Crowbar resistance	$R_{ds}/m\Omega$	200
Voltage	Us/kV	0–25

inductor (L) and a resistor (R). To alleviate the temperature increase in the coil, a crowbar circuit, comprised of a resistor (R_{ds}) and a diode (D_s), is inserted in parallel with the capacitor [30]. The capacitance is set as 160 µF, while the maximum discharge voltage can reach up to 25 kV, and more details about discharge parameters are provided in Table 2.

2.4 Numerical model

In this work, two numerical software, COMSOL and LS-DYNA, are applied, where the former is used to design the coil, while the latter is used to study the tube deformation processes. Figure 5a shows the two-dimensional axisymmetric simulation model built by COMSOL, which couples the electric and magnetic fields by finite element method (FEM). Figure 5b shows the full simulation model built by LS-DYNA coupling the electric field and magnetic field, as well as the structure field, which is mainly solved by finite element method (FEM) and boundary element method (BEM).

To build the stress-strain relationship for AA6061-O aluminum alloy, a uniaxial tensile test was performed. The obtained tensile test data is illustrated in Fig. 6, and the fitted quasi-static stress-strain curve, designated as σ_{qs}-ε, can be represented as follows:

$$\sigma_{qs} = 120.14\varepsilon^{0.157} \tag{4}$$

The significance of strain rate in affecting material flow stress is widely acknowledged. Therefore, the Cowper-Symonds constitutive model was utilized to characterize and address the strain rate effect, and it can be described as follows:

$$\sigma = \sigma_{qs}\left[1 + \left(\frac{\varepsilon_P}{P}\right)^m\right] \tag{5}$$

where ε_p represents the plastic strain rate, with specific values for P and m set at 6500 s^{-1} and 0.25 for aluminum [31], respectively. More details regarding the used materials can be found in Table 3.

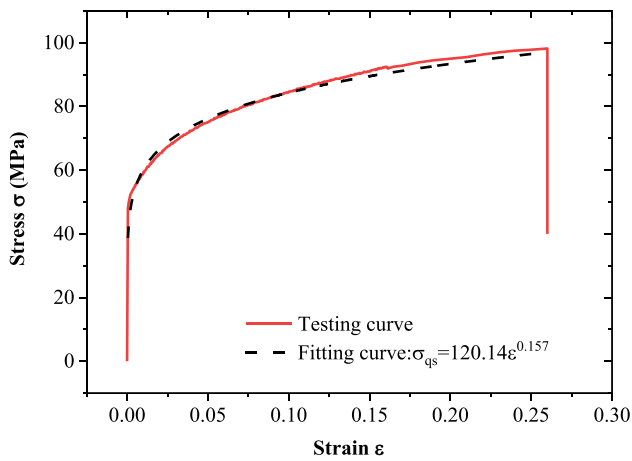**Fig. 5** Developed numerical model by COMSOL (**a**) and LS-DYNA (**b**)
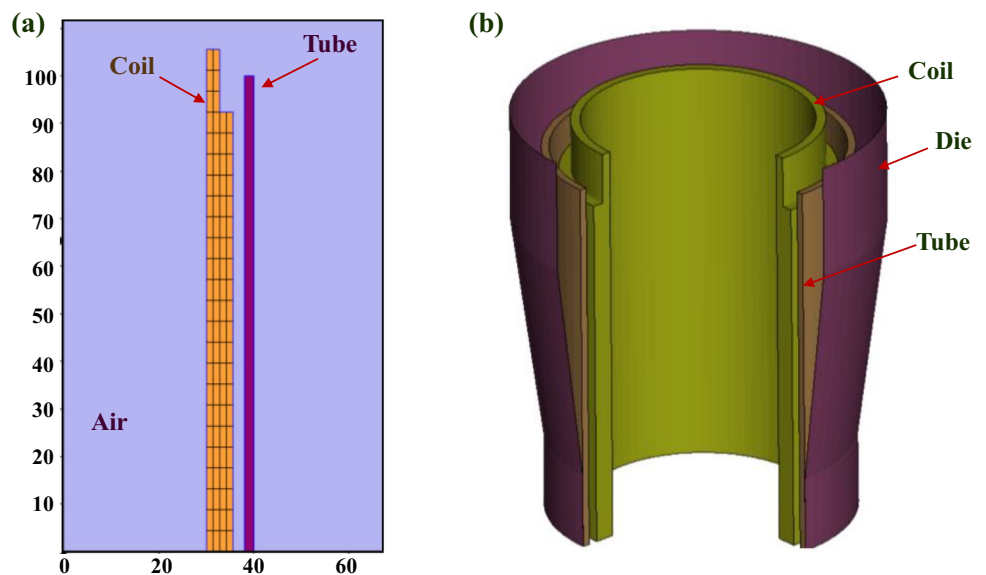
Fig. 6 Testing and fitting stress-strain curves of 6061-O tube

2.5 Experimental setup

Figure 7a illustrates one set of the power supply, comprising the capacitors, charger and switch, capable of achieving maximum capacitance and maximum voltage levels of 3.2 mF and 25 kV, respectively. Figure 7b shows the configuration of the forming device, including the coils, the tube, and the die. For ease in extracting the deformed tube, the die was manufactured in a splice mode. For further analysis, two specific paths along the length of the tube were selected.

3 Result and discussion

3.1 Implementation of the segmented coil

In this section, the effect of the segmented coil structure on the Lorentz force distribution is primarily discussed. Additionally, the strength of the segmented coil is calibrated through COMSOL, and finally, the winding method of the segmented coil is introduced.
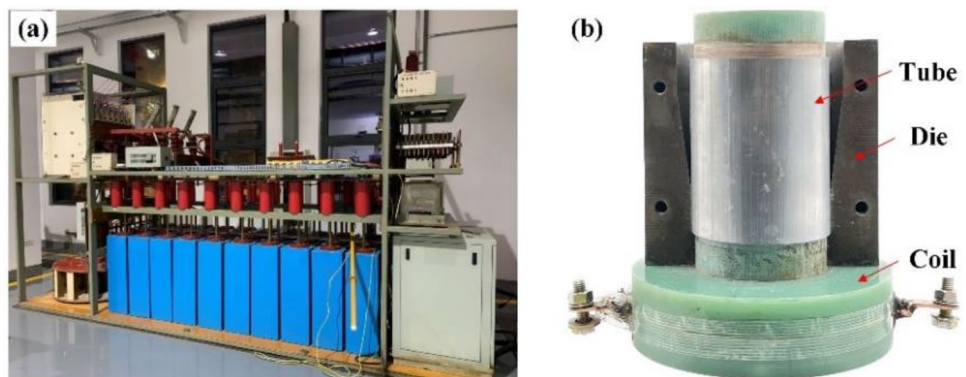
3.1.1 Design of the coil structure

Three cases are mainly considered in this section: (I) the conventional multi-layer coil, or coil with 0 turns reduced; (II) segmented coil with 6 turns reduced, as shown in Fig. 3c; and (III) segmented coil with 10 turns reduced. Figure 8 gives the coil currents under the three cases with the application of a 160 μF capacitance and a 10 kV discharge voltage. It is found that the segmented coil exhibits a shorter rising edge and a greater amplitude in the current waveform. This can be attributed to the lower resistance and inductance of the coil in the segmented configuration.

Figure 9 illustrates the distribution of the Lorentz force along the tube length. In each case, the tube remains fixed without undergoing deformation, and observations are made at the moment when the currents reach their peak values. It is evident that the force acting on the middle section of the tubes increases as the number of wire turns decreases. This can be attributed to the higher coil current associated with fewer turns. Regarding the force applied to the upper

Table 3 Mechanical and electrical properties of the used materials

Parameters	Materials		
	Tube (6061-O)	Die (304 steel)	Coil (copper)
Poisson ratio	0.33	0.29	0.34
Elastic modulus (GPa)	68.8	193	126
Yield strength (MPa)	55	215	80
Electrical resistivity ($\Omega \times m$)	3.66×10^{-8}	7.2×10^{-7}	1.66×10^{-8}

Fig. 7 Photos of the power supply (**a**) and forming devices (**b**)
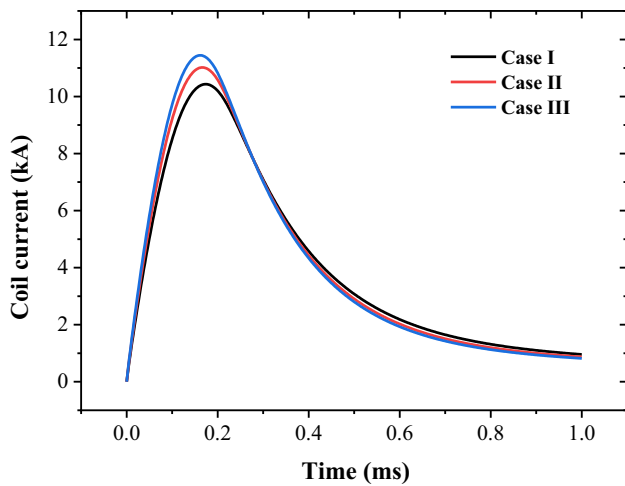
Fig. 8 Discharge current under the three cases

3.1.2 Analysis of the coil strength

Figure 11 illustrates the maximum effective stress and strain experienced by the coil at a capacitance of 160 μF and a discharge of 10 kV. It can be observed that the maximum stress in the coil is only 175 MPa, significantly lower than the ultimate stress capacity of 4 GPa that Zylon fiber can withstand. Additionally, the strain generated in the conductor after a single discharge can be ignored, indicating that the proposed segmented coil structure meets the discharge requirements.

3.1.3 Manufacturing process of the coil

Figure 12 illustrates the winding method employed for the segmented coil. The initial two layers are wound in a manner similar to that of a conventional coil. However, when the third layer begins to be wound, an epoxy ring is introduced at the end of the coil. For the segmented coil, reducing even-number layers (2 layers in this work) is recommended to ensure wires enter and exit the same port, which facilitates subsequent assembly of the copper electrodes. Following the wire winding process, the coil is further reinforced sequentially with Zylon and glass fibers. It is noteworthy that the coil has an outer diameter of 76 mm that matches the inner diameter of the tube. According to the above description, this winding method is very flexible and allows to generate different Lorentz force distributions to meet different forming conditions, such as forming variable-diameter tubes with different size.

section of the tube, it is noteworthy that when a conventional coil is employed, the force is greater than that in the middle section. However, this force diminishes when the number of wire turns in the upper section of the coil is decreased, and the extent of this reduction becomes more pronounced as the number of turns decreases further. To prevent insufficient Lorentz force generated in the upper portion of tubes, this study adopts the segmented coil structure presented in Case II.

Figure 10 illustrates the axial magnetic field density (B_z) and circumferential eddy current (J_{phi}) generated by a conventional coil and a segmented coil. Notably, the employment of a segmented coil results in a substantial reduction in both the magnetic field and eddy currents at the top end of the tube. Specifically, there is a 45% reduction in the magnetic field and a 33% reduction in eddy currents, signifying that both factors contribute significantly to the weakening of the Lorentz force in this configuration.

3.2 Verification of the proposed EMF process

In this section, the deformation process and forming quality of tubes by a conventional coil and the developed segmented coil are studied and compared.

Fig. 9 Distribution of Lorentz force along the tube length in the three cases

Fig. 10 Distribution of axial magnetic (**a**) and circumferential eddy current (**b**) along the tube length in the three cases
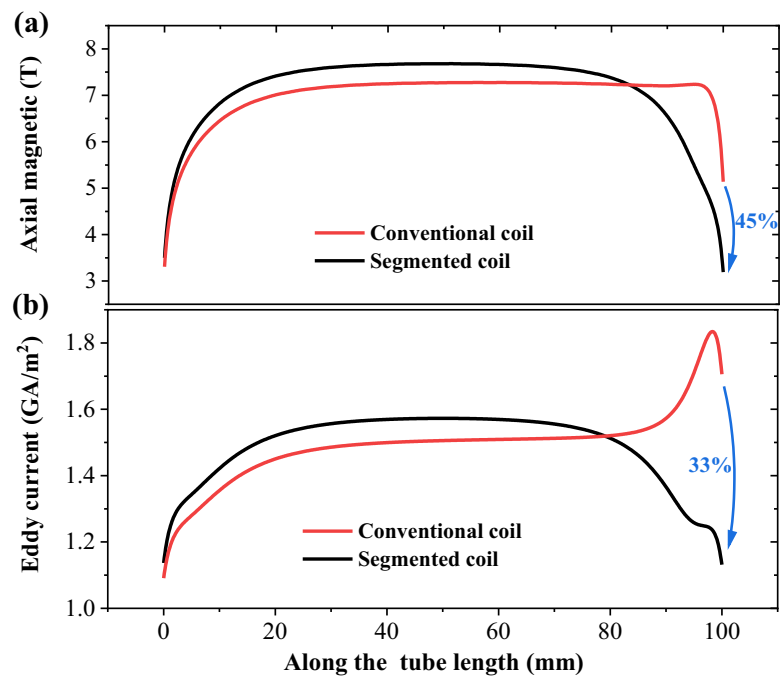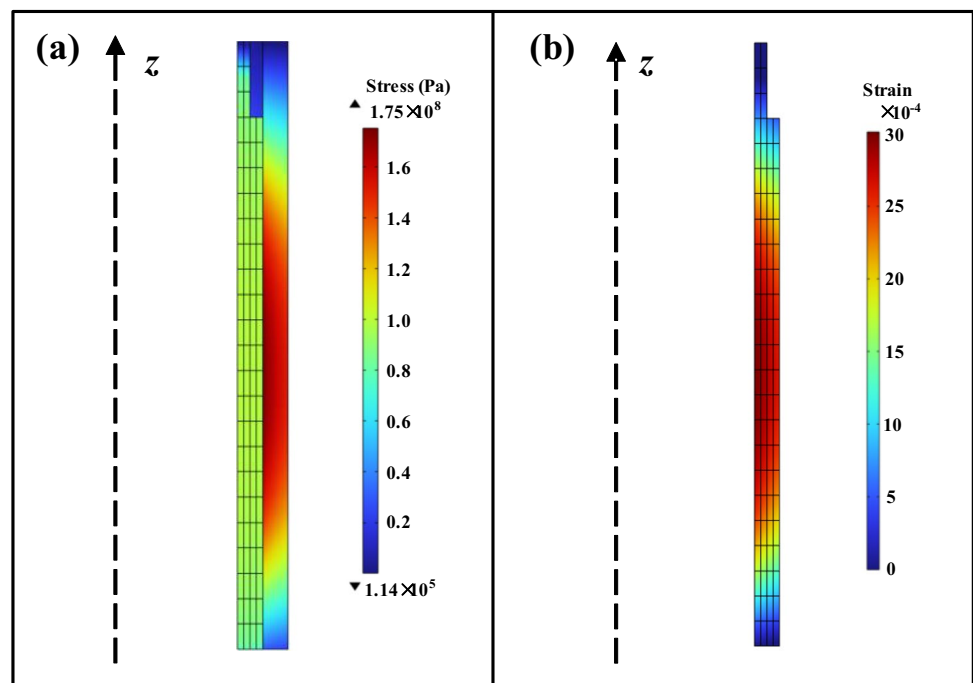

Fig. 11 Distribution of the maximum effective stress (**a**) and effective strain (**b**) of coil

3.2.1 Forming by a conventional coil

Figure 13a depicts the simulated process of the tube by a conventional multi-layer coil at a discharge of 9 kV. In the initial deformation stages ($t = 20$ µs), a noticeable Lorentz force is applied to the top portion of the tube, making this section undergo deformation first, while the bottom gradually conforms to the die from bottom to top (see $t = 80$ and 120 µs). With further deformation, the top portion of the tube contacts the die, creating a gap between the die and tube where trapped air cannot escape, hindering further tube deformation (see $t = 150$ µs). In the experiment, it is observable that there is a gap measured to be 1.6 mm between the tube and the die, and this gap persists despite any increase in voltage, as illustrated in Fig. 13b. These findings indicate that the primary factor contributing to the low forming quality of tube using a multi-layer solenoid coil is analogous to that observed with a single-layer solenoid coil.
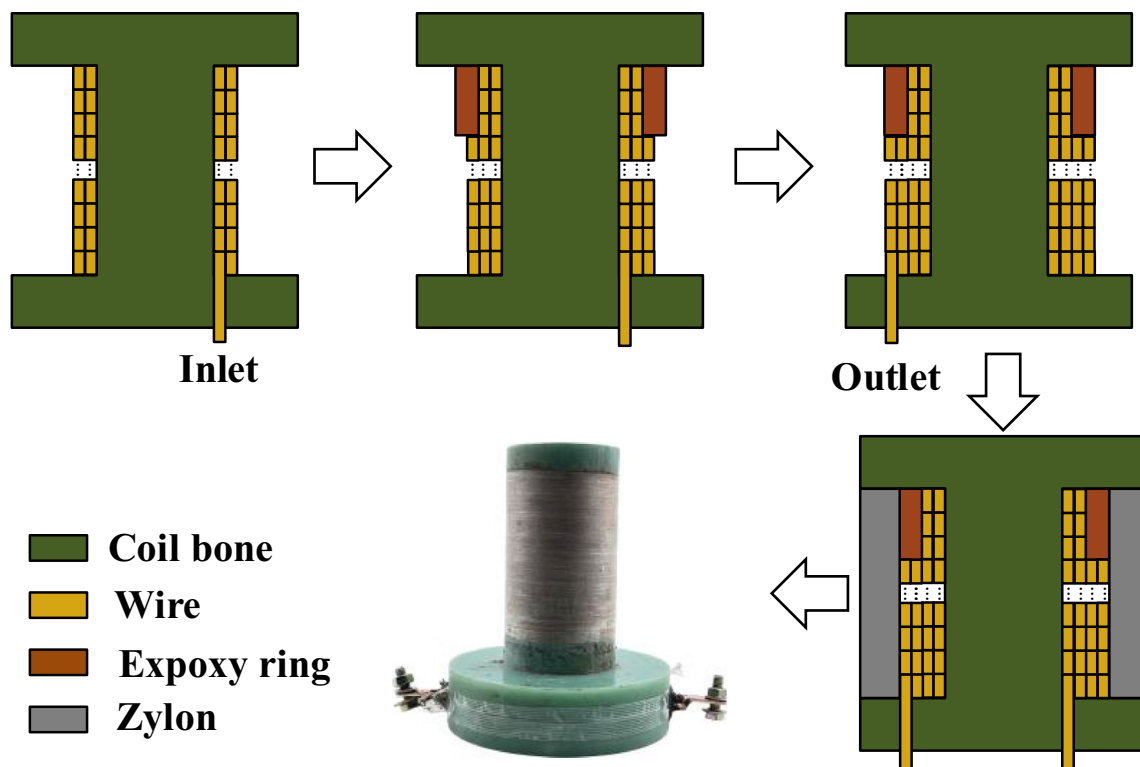
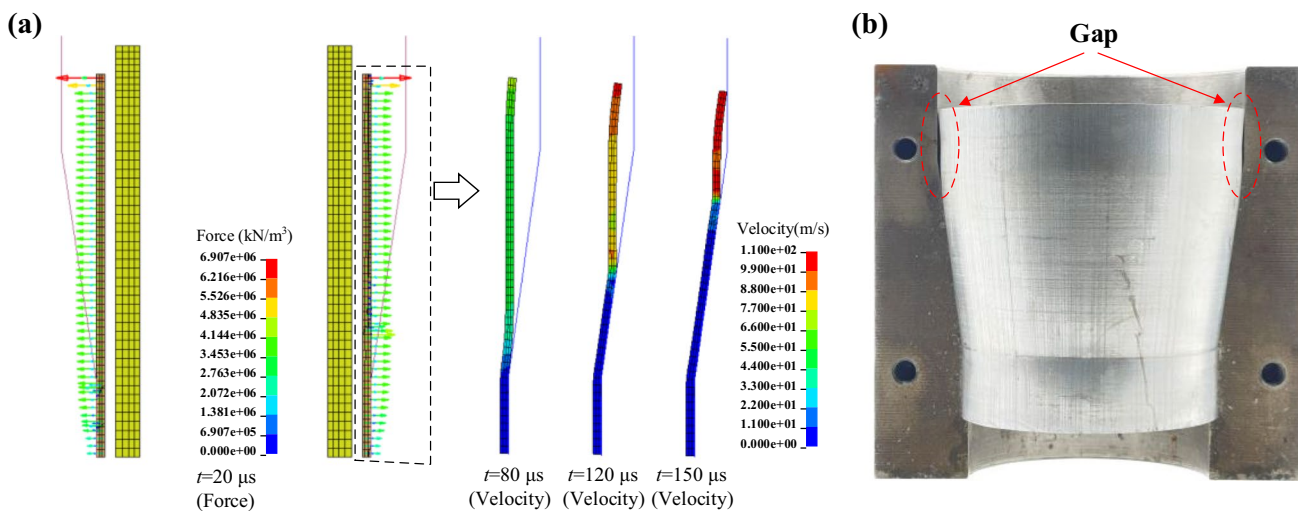**Fig. 12** Manufacturing process of the segmented coil

Fig. 13 Simulated deformation process of the tube (**a**) and photo of the deformed tube (**b**) under a conventional coil

3.2.2 Forming by a segmented coil

Figure 14 illustrates the tube deformation process using a segmented coil at a discharge of 10 kV. During the initial forming process, it is observed that the top portion of the tube experiences lower Lorentz forces (see $t = 20$ μs). Under this force, the central portion of the tube initiates deformation and gradually conforms to the die, progressing from the bottom to the top. As the Lorentz force and inertia effects continue to exert their influence, the remaining part of the tube is seen to progressively match the die from the bottom to the top during the intermediate phases (see $t = 140$ μs). Finally, a local cavity gap that could have hindered the forming process is eliminated, allowing the tube

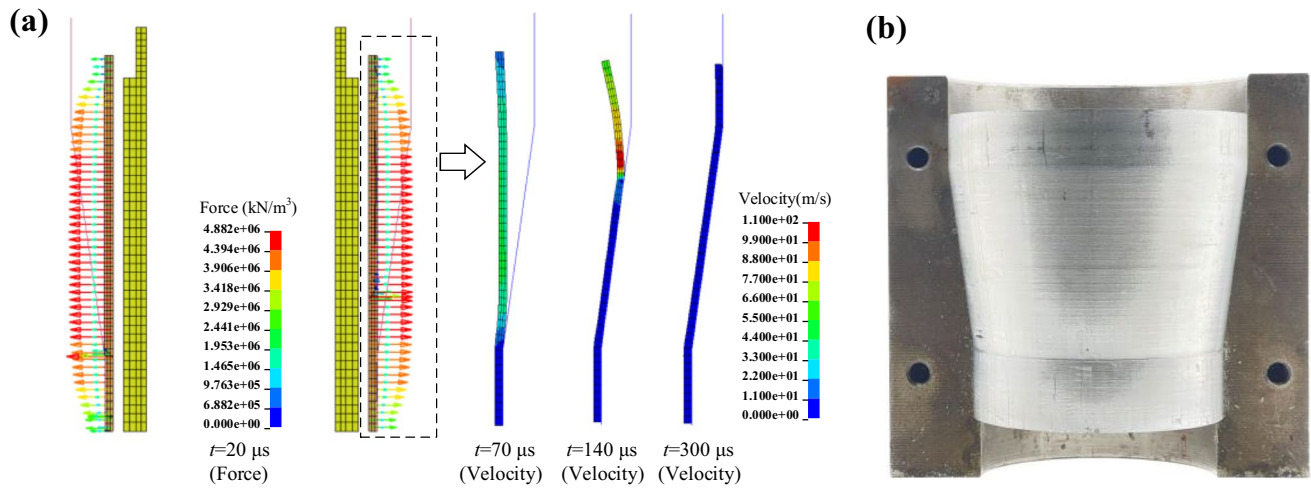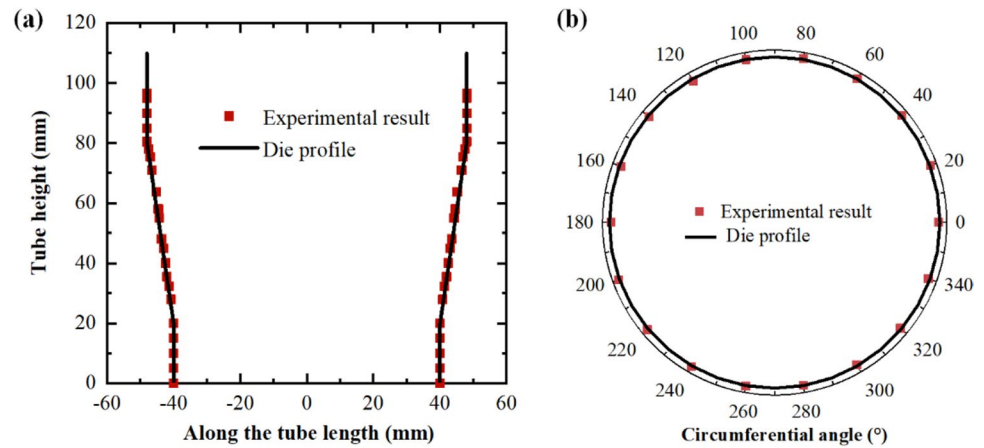**Fig. 14** Simulated deformation process of the tube (**a**) and photo of the deformed tube (**b**) under a segmented coil

Fig. 15 Measured die-fitting gap of the cross-section (**a**) and along the top circumferential direction (**b**)

to successfully conform to the die with a maximum gap of no more than 0.1 mm (see $t = 300$ μs).

Figure 15 displays the fitting accuracy of the tube in cross-section and along the top circumferential direction. It can be observed that the tube fits well with the die in any direction, affirming the efficacy of the proposed method in enhancing the forming accuracy of variable-diameter tubes.

3.3 Effect of system parameters on forming performance

In this section, the influence of discharge voltage and coil structure on the forming performance of tubes is discussed. Figure 16a illustrates the gap between the tube and the die at various discharge voltage levels with a capacitance fixed at 160 μF. It can be observed that the fitting performance is poor when the discharge voltage is low, which is due to the fact that the generated Lorentz force is insufficient to make the tube conform to the die,

especially for the upper section of the tube, as shown in Fig. 16b. This deformation shape also corresponds to the distribution of Lorentz forces. As the discharge voltage is raised to 10 kV, the tube matches closely with the die, and the fitting performance does not deteriorate with further increases in voltage.

Figure 17 displays the forming precision of tubes under different coil structures, with a fixed discharge voltage of 10 kV and a fixed capacitance of 160 uF. It can be observed that reducing the number of coil turns too few or too many both results in poor forming precision of the tubes. The former is due to the less apparent weakening of Lorentz force on the upper portion of tubes, leading to an unwanted gap, as shown in Fig. 13(b). The latter is because the excessive weakening of Lorentz force prevents it from conforming to the die, as illustrated in Fig. 16(b). Therefore, there exists an optimal coil structure that yields the best forming performance for the variable-diameter tube when the discharge energy is fixed.
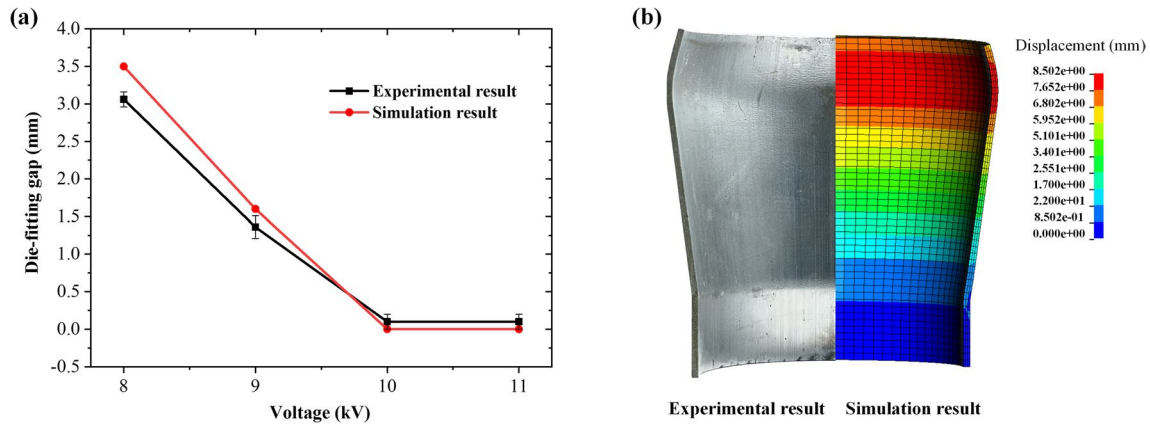
Fig. 16 Effect of voltage on die-fitting performance (**a**) and experimental and simulation results under a discharge of 8 kV (**b**)
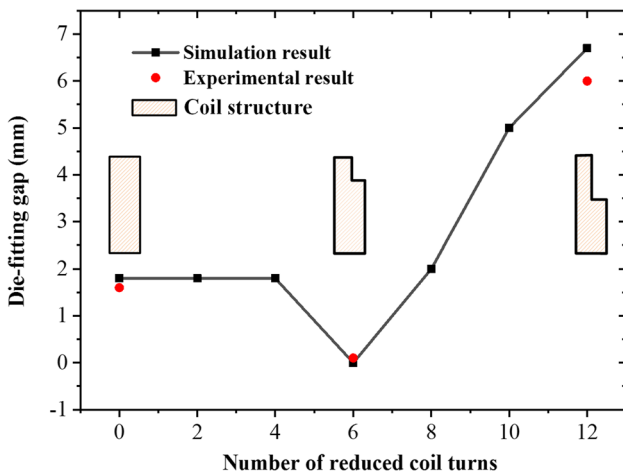

Fig. 17 Effect of coil structure on die-fitting performance

4 Conclusion

To overcome the problem of poor forming precision in variable-diameter tubes by conventional electromagnetic forming, this paper introduces an electromagnetic forming process using a segmented coil, and the primary findings can be summarized as follows:

(1) It is found that the use of a multi-layer solenoid coil can also cause excessive Lorentz force on the upper section of tubes, causing a gap that traps the air to cause poor forming performance of the tube, which is similar to that using a single-layer coil.

(2) It is found that the use of a segmented coil can reduce the force on the upper portion of tubes, thereby achieving a deformation process from bottom to top and obtaining a maximum gap of no more than 0.1 mm for tubes.

(3) It is found that the forming performance increases as the discharge voltage increases, and there exists an optimal coil structure for the best forming performance of tubes.

More applications of tube forming using a segmented coil will be explored in our future work.

Data availability Not applicable.

Declarations

Ethical approval Not applicable.

Consent to participate Not applicable.

Consent for publication All authors have read and agreed to the published version of the manuscript.

Competing interests The authors declare no competing interests.

References

1. Han C, Feng H (2020) Circumferential material flow in the hydroforming of overlapping blanks. Metals 10:864
2. Risch D, Psyk V, Tekkaya AE (2009) Investigation on a deep drawing and in-process electromagnetic calibration. Steel Res Int 80:329–334
3. Ouyang S, Du L, Li C, Li X, Wu Z, Lai Z, Han X, Cao Q, Li L (2023) Electromagnetic attractive forming of aluminum alloy tubes utilizing a dual-frequency current: new circuit design and forming process analysis. J Mater Process Technol 318:118006
4. Psyk V, Risch D, Kinsey BL, Tekkaya AE, Kleiner M (2011) Electromagnetic forming-a review. J Mater Process Technol 211:787–829

5. Xiao A, Yan Z, Huang C, Wang S, Long Z, Cui X (2022) Effect of initial state on formability of AA1060 alloy under quasi-static and electromagnetic forming. J Mater Res Technol 19:2781–2793

6. Liu W, Wu J, Liu J, Meng Z, Li J, Huang S (2023) Comparison of electromagnetic-driven stamping and electromagnetic forming limit curves for AA5182-O aluminum alloy sheet. Int J Adv Manuf Technol 126:2567–2577

7. Cui X, Zhang Z, Yu H, Xiao X, Cheng Y (2019) Springback calibration of a U-shaped electromagnetic impulse forming process. Metals 9:603

8. Li J, Qiu W, Huang L, Su H, Tao H, Li P (2018) Gradient electromagnetic forming (GEMF): a new forming approach for variable-diameter tubes by use of a sectional coil. Int J Mach Tools Manuf 135:65–77

9. Cao Q, Han X, Lai Z, Zhang B, Zhou Z, Qiu L, Li L (2014) Effects of current frequency on electromagnetic sheet metal forming process. IEEE Trans Appl Supercond 24:1–4

10. Cao Q, Xia L, Li X, Du L, Lai Z, Han X, Li L (2022) The importance of coil conductivity and eddy current effects in the analysis of electromagnetic forming process. High Volt 7:390–404

11. Paese E, Geier M, Homrich RP, Rosa P, Rossi R (2019) Sheet metal electromagnetic forming using a flat spiral coil: experiments, modeling, and validation. J Mater Process Technol 263:408–422

12. Qiu L, Yu Y, Xiong Q, Deng C, Cao Q, Han X, Li L (2018) Analysis of electromagnetic force and deformation behavior in electromagnetic tube expansion with concave coil based on finite element method. IEEE Trans Appl Supercond 28:1–5

13. Dond S, Choudhary H, Dikshit B, Kolge T, Sharma A (2020) Current frequency effect on electromagnetic tube expansion. Proc Inst Mech Eng Part C-J Eng Mech Eng Sci 234:4636–4644

14. Xiong Q, Tang H, Wang M, Huang H, Qiu L, Yu K, Chen Q (2019) Design and implementation of tube bulging by an attractive electromagnetic force. J Mater Process Technol 273:116240

15. Chen M, Lai Z, Cao Q, Han X, Wang C, Liu N, Li L (2020) Improvement on formability and forming accuracy in electromagnetic forming of deep-cavity sheet metal part using a dual-coil system. J Manuf Process 57:209–221

16. Chaharmiri R, Arezoodar AF (2017) The effect of stepped field shaper on magnetic pressure and radial displacement in electromagnetic inside bead forming: experimental and simulation analyses using maxwell and abaqus software. J Manuf Sci Eng-Trans ASME 139:061003

17. Yan Z, Xiao A, Zhao P, Cui X, Yu H, Lin Y (2022) Deformation behavior of 5052 aluminum alloy sheets during electromagnetic hydraulic forming. Int J Mach Tools Manuf 179:103916

18. Huang L, Ding Z, Zhou Y, Zeng J, Zou J (2020) Effect of the radial dimension of the driver sheet on the electromagnetic driven forming. IEEE Access 8:133503–133513

19. Xiong Q, Tang H, Deng C, Li L, Qiu L (2018) Electromagnetic attraction-based bulge forming in small tubes: fundamentals and simulations. IEEE Trans Appl Supercond 28:1–5

20. Xiong Q, Yang M, Liu X, Song X, Qiu L, Jiang J, Yu K (2020) A dual-coil method for electromagnetic attraction forming of sheet metals. IEEE Access 8:92708–92717

21. Ouyang S, Li X, Li C, Du L, Peng T, Han X, Li L, Lai Z, Cao Q (2020) Investigation of the electromagnetic attractive forming utilizing a dual-coil system for tube bulging. J Manuf Process 49:102–115

22. Kamal M, Daehn GS (2007) A uniform pressure electromagnetic actuator for forming flat sheets. J Manuf Sci Eng-Trans ASME 129:369–379

23. Wu Z, Cao Q, Fu J, Li Z, Wan Y, Chen Q, Li L, Han X (2020) An inner-field uniform pressure actuator with high performance and its application to titanium bipolar plate forming. Int J Mach Tools Manuf 155:103570

24. Oliveira DA, Worswick MJ, Finn M, Newman D (2005) Electromagnetic forming of aluminum alloy sheet: free-form and cavity fill experiments and model. J Mater Process Technol 170:350–362

25. Cui X, Zhang Z, Yu H, Cheng Y, Xiao X (2019) Dynamic uniform deformation for electromagnetic uniaxial tension. Metals 9:425

26. Soni M, Ahmed M, Panthi SK, Kumar S (2022) Effect of coil design parameters on performance of electromagnetic forming process. Mater Manuf Process 37:64–80

27. Qiu L, Li Y, Yu Y, Abu-Siada A, Xiong Q, Li X, Li L, Su P, Cao Q (2019) Electromagnetic force distribution and deformation homogeneity of electromagnetic tube expansion with a new concave coil structure. IEEE Access 7:117107–117114

28. Ouyang S, Xu X, Li X, Lai Z, Han X, Cao Q, Li L (2022) Systematic investigation of deformation behavior of tubes in a three-coil electromagnetic forming process. Int J Adv Manuf Technol 119:5163–5174

29. Ouyang S, Zhang W, Du L, Li C, Zhu X, Li X, Lai Z, Han X, Cao Q, Li L (2023) Enhancing forming accuracy in aluminum alloy variable-diameter tubes through dual-coil controllable electromagnetic forming. J Manuf Process 108:126–140

30. Cao Q, Han X, Lai Z, Xiong Q, Zhang X, Chen Q, Xiao H, Li L (2015) Analysis and reduction of coil temperature rise in electromagnetic forming. J Mater Process Technol 225:185–194

31. Mamalis AG, Manolakos DE, Kladas AG, Koumoutsos AK (2006) Electromagnetic forming tools and processing conditions: numerical simulation. Mater Manuf Process 21:411–423